Appendix A

Supplementary data

Table A.1 Statistical analysis of particle size (Y_1) and% entrapment efficiency (Y_2)in the Box-Behnken design

Term	Particle Size (Y_1)		%Entrapment Efficiency (Y_2)	
	Coefficient	*p*-value	Coefficient	*p*-value
Constant	+238.13	-	+75.70	-
X_1	18.92	0.0064*	15.12	<0.0001***
X_2	21.94	0.0034*	4.24	0.0042**
X_3	20.64	0.0045*	16.56	<0.0001***
X_1X_2	-11.15	0.1199	10.51	0.0003**
X_1X_3	0.2	0.9745	8.47	0.0009**
X_2X_3	35.02	0.0020*	-6.95	0.0022*
X_1^2	25.97	0.0086*	-10.15	0.0005**
X_2^2	10.60	0.1479	-10.53	0.0004**
X_3^2	-0.95	0.8836	-17.90	<0.0001***

*significant values at p<0.05, **significant values at p<0.001, *** significant values at p<0.0001

Table A.2 Model summary statistics of the quadratic response surface models for particle size (Y_1) and% entrapment efficiency (Y_2)

Response Variable	Quadratic Model							
	F-value	Prob>F[$]	R^2	Adj. R^2	Pred. R^2	Adeq. Prec.	C.V. (%)	Lack of Fit
Y_1	14.38	0.0045**	0.9628	0.8959	0.4607	11.722	4.63	0.1591[#]
Y_2	130.14	<0.0001***	0.9957	0.9881	0.9366	34.635	4.38	0.1159[#]

Adj. R^2, Adjusted R^2; Pred. R^2, Predicted R^2; Adeq. Prec., Adequate Precision; C.V., Coefficient of Variation

[$]Prob>F is the significance level, *significant values at p<0.05, **significant values at p<0.001, *** significant values at p<0.0001, [#]not significant

Table A.3 Actual and predicted values of particle size and % EE for check point analysis

Check point Batch code	X_1	X_2	X_3	Predicted value		Experimental Value		% Bias*	
				Particle size (nm)	%EE	Particle size (nm)	%EE		
CP 1	-0.5	-0.5	-0.5	221.06	48.99	205.2±4.7	45.57±4.2	7.17	6.98
CP 2	0.5	0.5	0.5	243.06	60.34	223.6±13.05	61.59±1.38	8.00	2.07
CP 3	-0.66	0.67	-0.69	292.64	84.28	299.3±3.1	89.57±0.431	-2.27	-6.27

*Bias was calculated as [(predicted value-experimental value)/predicted value] X 100.

All data are shown as mean ±S.D; n=3

Figures

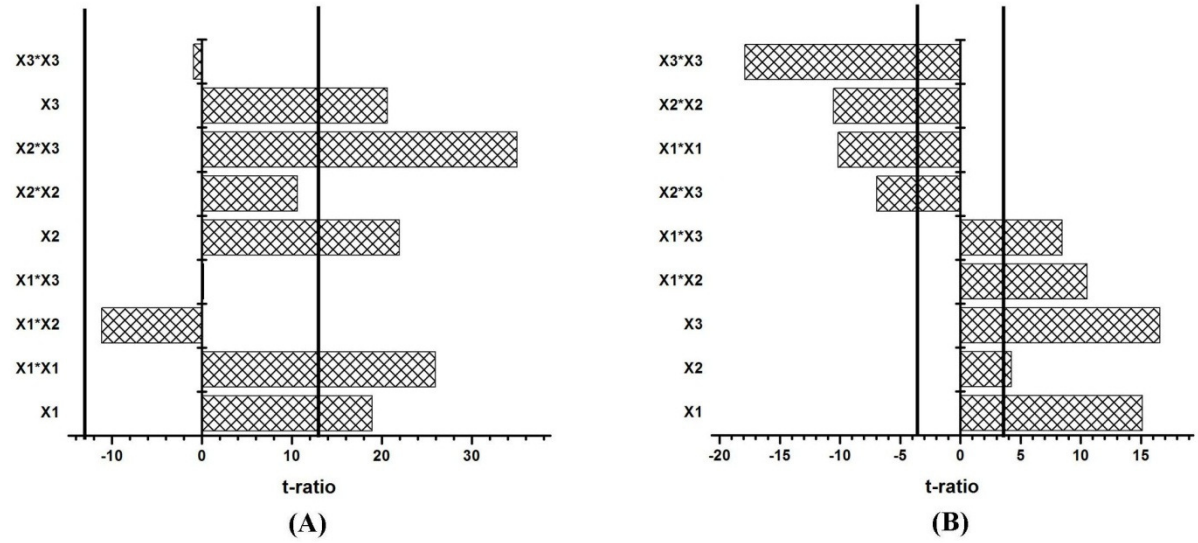

Fig. A.1 Pareto chart showing the quantitative effect of different formulation variables and their interaction on particle size (A) and % drug entrapment efficiency (B). The x-axis shows the standardized effect (t-ratio) of the variables; barsextending beyond the vertical line indicate values reaching statistical significance (p<0.05)

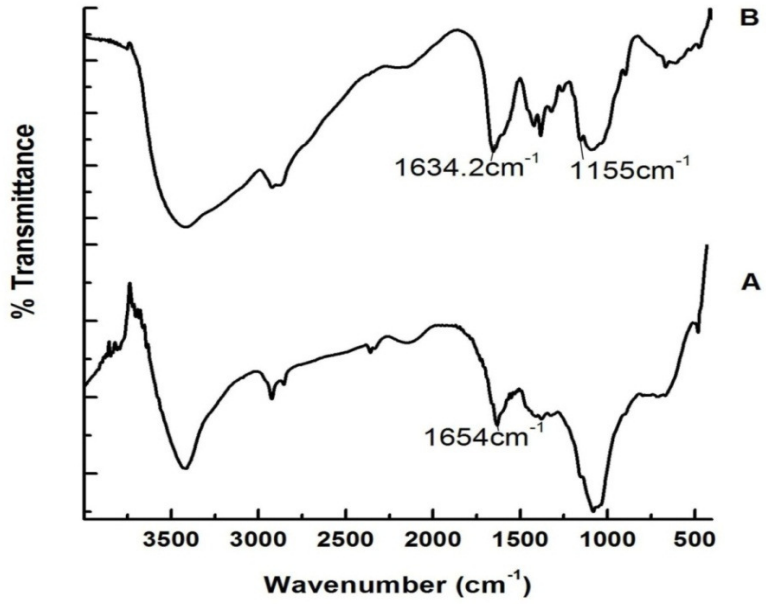

Fig. A.2 FTIR spectra of (A) chitosan and (B) crosslinked chitosan

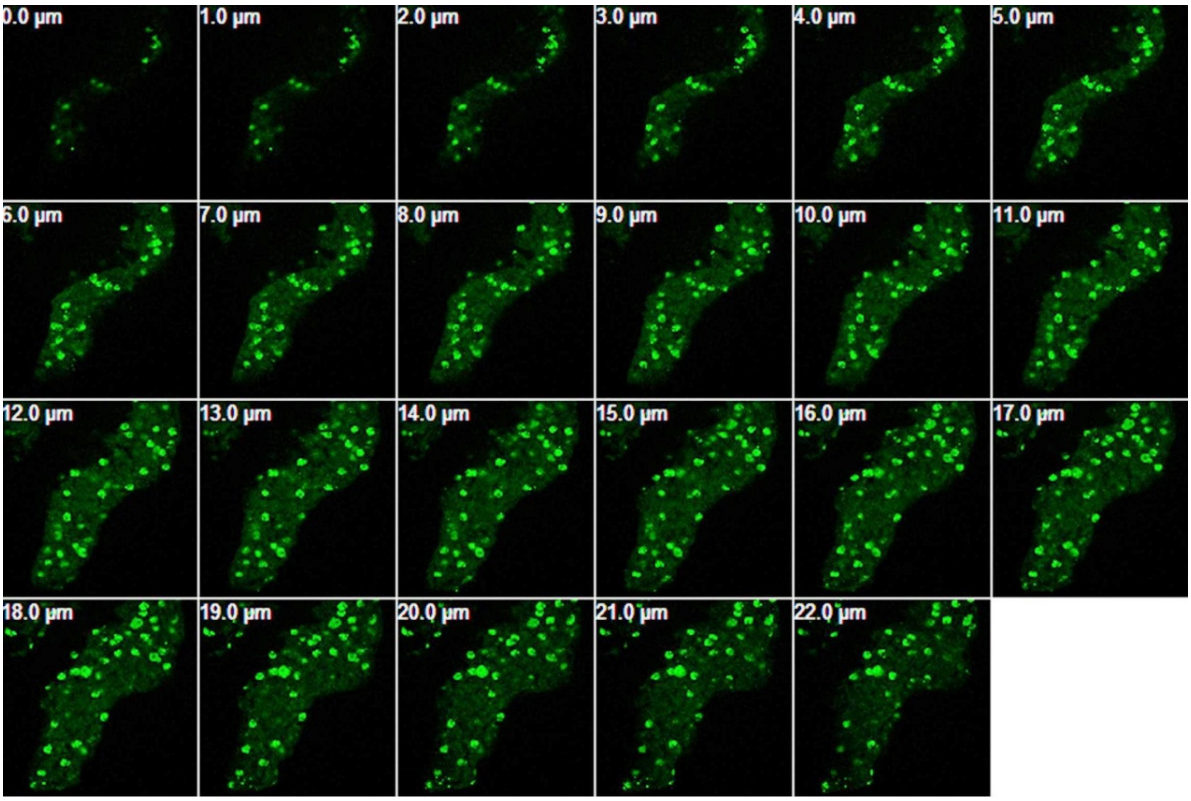

Fig. A.3 Three dimensional (3D) confocal images optically sectioned in the x-y plane at regularly spaced distances along the z-axis showing internalization of FITC-SCG-CSNPs in the intestinal villi.The top images represent sections closest to the apical membrane of cells, and the bottom images are the intracellular space toward basolateral side.

Lyophilization of SCG-CSNPs

Lyophilization of SCG-CSNPs was carried out on benchtop K freeze dryer (Virtis, 4KBTZL/105, USA). The nanoparticle dispersion with 1% mannitol as cryoprotectant was frozen at -60ºC for 3 hr in a deep freezer and then subjected to freeze drying. Sublimation lasted for 24 hr at a vacuum pressure of 100 milli torque without heating at room temperature, with the condenser surface temperature maintained at -100ºC. Freeze dried nanoparticles were reconstituted by double distilled water followed by sonication for period of 1 min.

Result

Different properties of lyophilized SCG-CSNPs like physical appearance, reconstitution nature and size ratio (before and after freeze drying) were analyzed and given in Table 7. The freeze dried SCG-CSNPs were found to be soft, white, amorphous, fluffy, free flowing in nature and were easily redispersed to form SCG-CSNPs by mere normal manual shaking. There was no significant difference in particle size and %EE of SCG-CSNPs after freeze drying as compared to before freeze drying (p>0.05). Moreover, Sa/Sb (ratio of particle size after and before freeze drying) remained almost unity (1.089). The % yield of optimized batch was found to be 85.84%. The % drug loading was checked by direct method, by measuring the actual amount of SCG within the CSNPs and it was found to be 8.66 $\pm$ 0.6%.

Table A.4. Particle size, PDI and % EE after and before freeze drying

Before Freeze drying			After freeze drying			Ratio (Sa/Sb)
Particle size (nm)	PDI	%EE	Particle size (nm)	PDI	%EE	1.089
204.9 $\pm$ 2.3	0.096 $\pm$ 0.04	63.68 $\pm$2.03	223 $\pm$ 5.6	0.206 $\pm$ 0.1	62.8 $\pm$ 2.67	

All data are shown as mean ±S.D; n=3

Conductivity study and pH study

The conductivity study and pH study were performed to monitor the cross-linking reaction between chitosan and TPP. The change in conductivity and pH was measured after each ml of addition of TPP solution to the chitosan solution on the conductivity meter (CM 183, Elico) and the pH meter (EI 120, Elico), respectively.

Result

When chitosan is dissolved in acidic environment, the amino group becomes positively charged. TPP provides both hydroxyl and phosphoric ions in presence of water that additionally depends on pH of solution. As crosslinking reaction involves interaction between cations and anions, pH of the TPP solution significantly affect the extent and kind of cross-linking. At pH 3 of TPP solution only phosphoric ions were present whereas at pH 9 both phosphoric as well as hydroxyl ions were present which compete with each other for interaction with positively charged amino group of chitosan. The conductivity study was performed to investigate the nature of crosslinking with the change in the ionic species relative to change in pH. At lower pH (pH 3), conductivity decreased up to 5 ml due to interaction between amino group and phosphoric ion. Further, addition of TPP solution, conductivity increases after equivalence point attributable to saturation of amino group to chitosan and also due to increase of H^+ ions. Hence, the process was confirmed as preponderantly ionic crosslinking. Whereas at higher pH of TPP solution (pH 9), the decrease in conductance was seen up to 9 mL due to presence of both hydroxyl and phosphoric ions which compete with each other for positive amino group. The hydroxyl radical interacts with amino group by deprotonation (Fig. S.2A). Moreover, the results were additionally well explained by pH measurement. At higher pH (pH 9), gradual increase in pH was observed whereas at lower pH (pH 3), the pH of the system remains unchanged throughout crosslinking (Fig. S.2B). From the study it had been confirmed that at lower pH crosslinking

reaction proceed by ionic crosslinking whereas higher pH deprotonation and ionic crosslinking, each mechanisms exists.

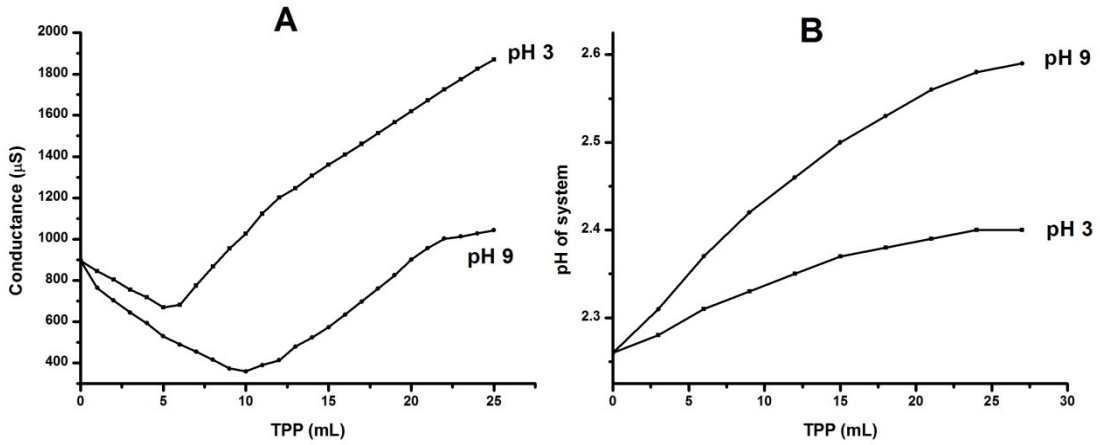

Fig. A.4. Effect of pH of TPP on (A) conductivity and (B) pH of the system during crosslinking of chitosan with TPP

Swelling index study

200 mg of freeze dried SCG-CSNPs were dispersed in 250 ml phosphate buffer (pH 6.8) for a period of 6 hr at room temperature. The swollen NPs were collected by centrifugation and the wet weight of the swollen CSNPs was recorded by first blotting with filter paper to remove excess water on the surface and then weighing immediately on electronic balance at predetermined time period (0.5, 1, 2, 3, 4, 5 and 6 h). Swelling index (SI) was then calculated using the following formula.

$$\text{Swelling index} = \frac{Ws - Wi}{Wi} \times 100$$

Where, Wi was the initial weight, Ws was the swollen weight

Result

Swelling study was carried out to assess the crosslinking density of the SCG-CSNPs as it directly affects the physical properties of SCG-CSNPs and thereby permeability and drug release behaviour. From the study it was found that swelling of the SCG-CSNPs was time dependent in phosphate buffer pH 6.8 as shown in Fig. S.4. A contrary relation observed between the swelling capacity and the crosslinking density of the CSNPs. The decrease in

swelling capacity with increase in the crosslinking density could be attributed to the more tightly crosslinked chitosan matrix that does not swell as compared to loosely packed chitosan matrix. At lower volume of crosslinking agent, the chitosan network loosely crosslinked and had high hydrodynamic free volume to accommodate more solvent molecules thereby inducing CSNPs matrix swelling. The water uptake and thereby swelling in hydrogels depends upon the extent of hydrodynamic free volume and accessibility of hydrophilic functional groups with which water can establish hydrogen bonds. As SCG-CSNPs shows lesser swelling compared to other available literature indicates that there was better crosslinking density in the SCG-CSNPs with tightly crosslinked matrix which provides structure rigidity and presence of less number of free hydrophilic groups in CSNPs that are responsible for swelling. Moreover, the obtained results also correlate that at neutral and basic pH, CSNPs formed by deprotonation mechanism and fewer amounts of phosphate groups involves in crosslinking process. As phosphate group imparts water holding capacity and thereby swelling property, due to presence of fewer amounts of phosphate groups in crosslinked SCG-CSNPs, it shows lesser swelling behaviour**.**

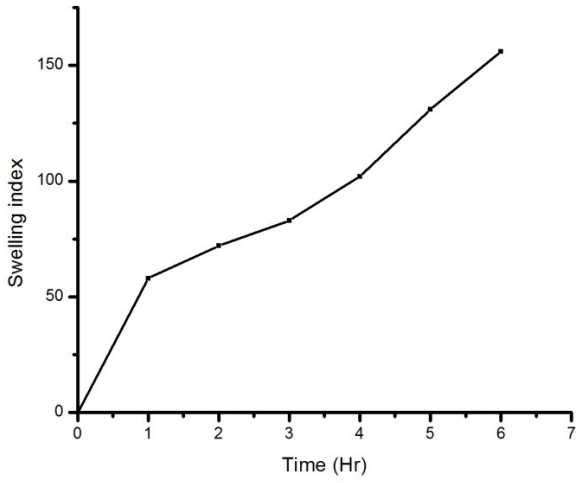

Fig. A.5. Swelling behaviour of SCG-CSNPs in phosphate buffer pH 6.8